# Modeling and Control of Contouring Errors for Five-Axis Machine Tools—Part II: Precision Contour Controller Design

**Burak Sencer**
Ph.D. Candidate

**Yusuf Altintas**
Professor
Fellow ASME

Manufacturing Automation Laboratory,
The University of British Columbia,
Vancouver, BC, V6T 1Z4, Canada

*The accurate tracking of tool-paths on five-axis CNC machine tools is essential in achieving high speed machining of dies, molds, and aerospace parts with sculptured surfaces. Because traditional CNCs control the tracking errors of individual drives of the machine, this may not lead to desired contouring accuracy along tool-paths, which require coordinated action of all the five drives. This paper proposes a new control approach where the tool tip and tool orientation errors, i.e., the contouring errors, are minimized along the five-axis tool-paths. The contouring error and kinematic model of the machine, which are presented in Part I of the paper, are used in defining the plant. A multi-input–multi-output sliding mode controller, which tries to minimize path tracking and path following velocity errors, is introduced. The stability of the system is ensured, and the proposed model is experimentally demonstrated on a five-axis machine tool. The path errors originating from the dynamics of five simultaneously active drives are significantly reduced.* [DOI: 10.1115/1.3123336]

## 1 Introduction

Contouring errors, defined as the normal deviation from the desired reference tool-path, occur in multi-axis motion control systems due to tracking errors of individual servo drives. In Part I of the paper, two types of *contour errors*, which are detrimental to the part tolerances during simultaneous five-axis machining, are defined. The first one is the normal deviation of the tool tip from the desired tool-path, called the *tool tip contour error*. Considering the kinematics of the five-axis machine tools, tool tip contour errors arise as a nonlinear function of the tracking errors of all the axis. *Orientation contour error*, on the other hand, is defined as deviation from the desired tool orientation in spherical coordinates and controlled only by the rotary drives of a five-axis machine tool. Models that accurately estimate both of those contour errors in real time are presented in Part I. The design of a simultaneous multi-axis sliding mode controller (SMC) for minimizing contour errors is introduced.

Two major approaches have been adopted to reduce contouring errors. In the first approach, contour errors are reduced indirectly, by attempting to reduce axis tracking errors. Traditional algorithms such as P, PI, and PID are based on the feedback principle [1,2]. Tomizuka [3] developed a zero phase error tracking controller (ZPETC) by canceling the stable dynamics of the servo drive in a feed-forward fashion. The bandwidth of the overall system, hence the tracking accuracy of the drive, increases with ZPETC, provided that the drive model is accurate and does not vary with time [4,5]. Recent efforts are directed toward improving the bandwidth of the drives using sliding mode controllers that are more robust to the changes in the drive dynamics. The general SMC was first introduced by Utkin [6], which required switching around the sliding surface resulting in a discontinuous control law. To overcome this problem, Slotine and Li [7] proposed an adaptive sliding mode controller, which estimates and cancels various uncertainties that do not vanish at the equilibrium point. In parallel, Stepanenko et al. [8] noted that the transient response of the discontinuous SMCs can be improved by including the integral, position, and derivative of the tracking errors in the sliding surface design. Later, Altintas et al. [9] proposed a continuous sliding mode controller for accurate tracking control of axis by considering only the rigid body dynamics of the ball screw drive. Their SMC design was based on panelizing position, as well as the velocity errors of the axes, and demonstrated similar performance to the ZPETC but with improved robustness to uncertainties in the drive dynamics.

An improved method of controlling the machine tool feed drive system is to introduce coupling actions in the controller to maintain coordination along the desired contour. By introducing coupling effects among multiple axes, coordinated motion is achieved by either the "equal status" or the "master-slave approach" [10]. When the dynamics are significantly different among multiple axis, the controller designed by the equal status approach may saturate the slower axis actuator. In order to overcome this drawback, the master-slave approach is favored, which assigns the slow axis as the master of the faster drive. Su et al. [11] developed an adaptive coordination controller for position synchronization of multiple axis. They defined the *synchronization error* as the differential position error among multiple motion axes and penalized it in the feedback loop [12].

The second major approach in reducing contour errors is to attempt to estimate contour errors in real time and generate control action against it. Koren and Lo [13] estimated the contouring error in two axis machines as a function of axis tracking errors and linear feed direction between consecutive path points. They reduced the contouring error by injecting corresponding coupling command to the servos in order to push the actual tool position on the desired tool-path, known as the cross coupled controller (CCC). Later, Koren and Lo [14] used time varying coupling gains to implement CCC along circular paths. When the axis controllers minimize the tracking errors along a curved path, the contour error is increased, which will force the contour controller to resist it. As a result, it is difficult to distinguish which control element dominates the final contouring result. The analysis hindered implementation of the CCC scheme in nonorthogonal machine tools. Erkorkmaz and Altintas [15] developed a numerical method to estimate the contour error for arbitrarily shaped tool-

**Table 1 Drive parameters**

| | $x$-axis (V s$^2$/mm) | $y$-axis (V s$^2$/mm) | $z$-axis (V s$^2$/mm) | $a$-axis (V s$^2$/rad) | $c$-axis (V s$^2$/rad) |
|---|---|---|---|---|---|
| $m = J/K_a K_t r_g$ | 0.00162 | 0.00174 | 0.00296 | 0.00682 | 0.00054 |
| $c = B/K_a K_t r_g$ | 0.00681 | 0.00863 | 0.01518 | 0.01964 | 0.00368 |

paths. They implemented it in a CCC scheme together with feedforward axis dynamics compensation and demonstrated improved contouring performance for Cartesian machining. Chiu and Tomizuka [16] used the coordinate transformation approach to directly design for the desired contour error dynamics. Using linear time varying PD regulators, the decoupled error dynamics in tangential and normal directions are stabilized. This approach demonstrated that the contouring performance is improved by increasing the closed loop bandwidth in the normal direction. However, the PD controller is not sufficiently robust enough, and the contour error approximation may become inaccurate. Therefore, the contouring accuracy degrades in speed machining of paths with sharp curvatures. Peng and Chen [17] defined a geometric contouring index (CI) that improves the error estimation on circular tool-paths and designed a back stepping sliding mode controller in the normal direction to introduce robustness against friction. Chen et al. [18] later designed robust controllers in polar coordinates to establish contouring control for very simple noncircular tool-paths.

A completely different philosophy is introduced in this paper. Rather then tracking of individual drives, the tool-path following the accuracy of five-axis machine tools, i.e., the *minimization of contouring error*, is considered as the prime objective of the control law. By utilizing the kinematic and contour error estimation models presented in Part I, a multi-input–multi-output (MIMO) continuous time integral sliding mode contour controller is introduced, which is more robust against disturbances and modeling errors. The effectiveness of the control strategy is demonstrated experimentally on the in-house controlled five-axis CNC machine tool.

This paper is organized as follows: Section 2 describes the design of sliding mode controllers for minimizing the tool tip as well as the tool orientation contour errors. Section 3 investigates the effectiveness of the control algorithms through contouring tests.

## 2 Contouring Control

The simplified linear dynamics of a typical feed drive system on a five-axis machine tool was modeled in Part I as

$$\ddot{\mathbf{q}}(t) = \mathbf{M}^{-1}[\mathbf{u}(t) - \mathbf{d}(t) - \mathbf{C}\dot{\mathbf{q}}(t)] \quad (1)$$

where $\mathbf{q}(t) = [x(t), y(t), z(t), \theta_a(t), \theta_c(t)]^T$ contains the drive positions. $\dot{\mathbf{q}}(t)$ and $\ddot{\mathbf{q}}(t)$ contain the drive velocities and accelerations, respectively. $\mathbf{u}(t)$ is the control input to the amplifiers and $\mathbf{d}(t)$ is the external disturbance reflected at the amplifier's input. $\mathbf{M} \in \mathfrak{R}^{5 \times 5}$ and $\mathbf{C} \in \mathfrak{R}^{5 \times 5}$ are the diagonal matrices that contain drives' equivalent inertia and viscous damping terms given in Table 1. The Jacobian matrix, $\mathbf{J}(t) \in \mathfrak{R}^{5 \times 5}$, relates drive velocities ($\dot{\mathbf{q}}(t)$) to the tool pose velocity ($\dot{\mathbf{x}}(t) = [\dot{P}_x(t), \dot{P}_y(t), \dot{P}_z(t), \dot{a}(t), \dot{c}(t)]^T$) and is obtained from the kinematics of the five-axis machine [19]. The drive dynamics are mapped to the tool pose using the Jacobian, and the tracking error dynamics of the tool in the workpiece coordinate system are expressed by

$$\ddot{\mathbf{e}}(t) = \ddot{\mathbf{x}}_{\text{ref}}(t) - \dot{\mathbf{J}}(t)\dot{\mathbf{q}}(t) - \mathbf{J}(t)\mathbf{M}^{-1}[\mathbf{u}(t) - \mathbf{d}(t) - \mathbf{C}\dot{\mathbf{q}}(t)] \quad (2)$$

where $\ddot{\mathbf{x}}_{\text{ref}}(t)$ is the reference tool pose acceleration. Based on the contour error and drive dynamics models presented in Part I [19], a sliding mode controller that minimizes both the tool tip and orientation contour errors is introduced in Sec. 2.1.

**2.1 Design of Sliding Mode Controller for the Tool Tip Contour Errors.** In Part I, the actual tool tip contour error vector ($\boldsymbol{\varepsilon}$) is modeled by reflecting the tool tracking tip errors ($\mathbf{e}$) on the delay compensated Frenet frame ($\widetilde{\mathbf{F}}$) as follows:

$$\left.\begin{array}{l} \widetilde{\mathbf{e}}_{\mathbf{F}} = \widetilde{\mathbf{F}}^{\mathbf{T}}\mathbf{e} + \widetilde{\mathbf{h}}_{\mathbf{F}} \\[4pt] \dot{\widetilde{\mathbf{e}}}_{\mathbf{F}} = \widetilde{\mathbf{F}}^{\mathbf{T}}\dot{\mathbf{e}} + \dot{\widetilde{\mathbf{F}}}^{\mathbf{T}}\mathbf{e} + \dot{\widetilde{\mathbf{h}}}_{\mathbf{F}} \\[4pt] \ddot{\widetilde{\mathbf{e}}}_{\mathbf{F}} = \widetilde{\mathbf{F}}^{\mathbf{T}}\ddot{\mathbf{e}} + 2\dot{\widetilde{\mathbf{F}}}\dot{\mathbf{e}} + \ddot{\widetilde{\mathbf{F}}}^{\mathbf{T}}\mathbf{e} + \ddot{\widetilde{\mathbf{h}}}_{\mathbf{F}} \end{array}\right\} \quad (3)$$

The contour errors left on the part surface are estimated from the normal and binormal components ($\vec{\boldsymbol{\varepsilon}} \cong \widetilde{\mathbf{e}}_{\mathbf{F,n}} + \widetilde{\mathbf{e}}_{\mathbf{F,b}}$) of the errors (Fig. 1), which are minimized by the sliding mode controller. The contour error dynamics are derived by substituting Eq. (2) into Eq. (3):

$$\ddot{\widetilde{\mathbf{e}}}_{\mathbf{F}} = \begin{bmatrix} \ddot{\tilde{e}}_t \\ \ddot{\tilde{e}}_n \\ \ddot{\tilde{e}}_b \\ \ddot{\tilde{e}}_a \\ \ddot{\tilde{e}}_c \end{bmatrix} = \widetilde{\mathbf{F}}^{\mathbf{T}}[\ddot{\mathbf{x}}_{\text{ref}} - \dot{\mathbf{J}}\dot{\mathbf{q}} - \mathbf{J}\mathbf{M}^{-1}(\mathbf{u} + \mathbf{d} - \mathbf{C}\dot{\mathbf{q}})] + 2\dot{\widetilde{\mathbf{F}}}^{\mathbf{T}}\dot{\mathbf{e}} + \ddot{\widetilde{\mathbf{F}}}^{\mathbf{T}}\mathbf{e} + \ddot{\widetilde{\mathbf{h}}}_{\mathbf{F}}$$

$$(4)$$

Note that the dynamics of the first three components, namely, the tangent, normal, and binormal ($\tilde{e}_t, \tilde{e}_n, \tilde{e}_b$) errors, are nonlinear and time varying due to the Jacobian and Frenet frame transformations. The last two components are regular tracking error dynamics of the rotary drives. A second order sliding surface ($\mathbf{S} \in \mathfrak{R}^{5 \times 1}$) is designed to contain the proportional, integral, and derivative of the time varying errors according to
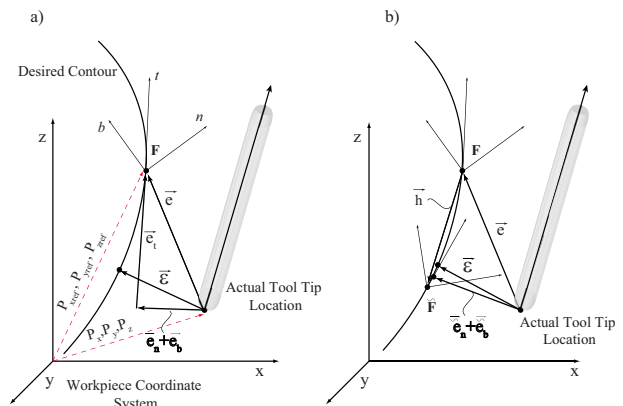


**Fig. 1 Tool tip contour error estimation**

$$\mathbf{S} = \begin{bmatrix} S_t \\ S_n \\ S_b \\ S_a \\ S_c \end{bmatrix} = \mathbf{C_P}\widetilde{\mathbf{e}}_F + \mathbf{C_I}\int_0^t \widetilde{\mathbf{e}}_F d\tau + \mathbf{C_D}\dot{\widetilde{\mathbf{e}}}_F \qquad (5)$$

where $\mathbf{C_P} \in \mathfrak{R}^{5\times5}$, $\mathbf{C_I} \in \mathfrak{R}^{5\times5}$, and $\mathbf{C_D} \in \mathfrak{R}^{5\times5}$ are the diagonal design matrices that represent the desired achievable dynamics of the errors on the sliding surface. The control input ($\mathbf{u} \in \mathfrak{R}^{5\times1}$) must be manipulated in such a way that the errors and the time derivative converge asymptotically to the stable sliding surface, so that they eventually slide to origin $\mathbf{S}\rightarrow\mathbf{0}$ as $\widetilde{\mathbf{e}}_F\rightarrow\mathbf{0}$ and $\dot{\widetilde{\mathbf{e}}}_F\rightarrow\mathbf{0}$. The error dynamics on the sliding surface can be represented in Laplace domain as

$$\dot{\mathbf{S}} = (\mathbf{C_D}s^2 + \mathbf{C_P}s + \mathbf{C_I})\widetilde{\mathbf{e}}_F(s) = 0 \qquad (6)$$

and stable second order error dynamics can be designed by choosing constant design matrices

$$\mathbf{C_D} = \mathbf{I}_{5\times5}$$

$$\mathbf{C_P} = \mathrm{diag}(2\zeta_t\omega_{n,t}, 2\zeta_n\omega_{n,n}, 2\zeta_b\omega_{n,b}, 2\zeta_a\omega_{n,a}, 2\zeta_c\omega_{n,c})$$

$$\mathbf{C_I} = \mathrm{diag}(\omega_{n,t}^2, \omega_{n,n}^2, \omega_{n,b}^2, \omega_{n,a}^2, \omega_{n,c}^2) \qquad (7)$$

where $\zeta_i$ and $\omega_{n,i}$, $i=t,n,b,a,c$ are the individual damping and natural frequencies for each tracking error component. The variation in the external disturbance caused by the cutting process and friction is considered to be constant and remains between the upper ($\mathbf{d}^+ \in \mathfrak{R}^{5\times1}$) and lower ($\mathbf{d}^- \in \mathfrak{R}^{5\times1}$) limits during short time intervals [9]. The external disturbances force contouring errors to deviate from the sliding surface, but they can be tracked using the following observer that integrates the sliding surface:

$$\dot{\hat{\mathbf{d}}} = \mathbf{\Gamma}\boldsymbol{\kappa}\mathbf{J}^T\widetilde{\mathbf{F}}\mathbf{S} \rightarrow \hat{\mathbf{d}}(k) = \hat{\mathbf{d}}(k-1) + T\mathbf{\Gamma}\boldsymbol{\kappa}\mathbf{J}^T\widetilde{\mathbf{F}}\mathbf{S} \qquad (8)$$

where $T$ is the control sampling period, $\mathbf{\Gamma} = \mathrm{diag}(\Gamma_t, \Gamma_n, \dots, \Gamma_c)$ is the observer gain matrix, $\mathbf{J}^T$ is the transpose of the Jacobian, and $\boldsymbol{\kappa} = \mathrm{diag}(\kappa_t, \kappa_n, \dots, \kappa_c)$ is a matrix with positive entries used to impose limits on the integral control action against the disturbances so that the observations are within the given bounds ($\mathbf{d}^- \leq \hat{\mathbf{d}} \leq \mathbf{d}^+$):

$$\boldsymbol{\kappa} = \begin{cases} 0 & \text{if } \hat{\mathbf{d}} \leq \mathbf{d}^- \quad \text{and} \quad \mathbf{S} \leq \mathbf{0} \\ 0 & \text{if } \hat{\mathbf{d}} \geq \mathbf{d}^+ \quad \text{and} \quad \mathbf{S} \geq \mathbf{0} \\ 1 & \text{otherwise} \end{cases} \qquad (9)$$

The bounded disturbance observer avoids chattering of the controller on the sliding surface. In order to push the tracking errors onto the sliding surface, the following Lyapunov vector function is postulated as

$$\mathbf{V} = \begin{bmatrix} V_t \\ V_n \\ V_b \\ V_a \\ V_c \end{bmatrix} = \frac{1}{2}\{\mathbf{S}^T\mathbf{M}\mathbf{S} + (\mathbf{d}-\hat{\mathbf{d}})^T\mathbf{\Gamma}^{-1}(\mathbf{d}-\hat{\mathbf{d}})\} \qquad (10)$$

This function panelizes the deviation from the surface and the square of the disturbance estimation error. The derivative of the Lyapunov function

$$\dot{\mathbf{V}} = \mathbf{S}^T\mathbf{M}\dot{\mathbf{S}} - (\mathbf{d}-\hat{\mathbf{d}})^T\mathbf{\Gamma}^{-1}\dot{\hat{\mathbf{d}}} \qquad (11)$$

must be negative for asymptotic stability, which also pushes the states toward the sliding surface where they follow the desired second order dynamics. Equations (6) and (8) are substituted into Eq. (11) to yield

$$\dot{\mathbf{V}} = \mathbf{S}^T\mathbf{M}[\mathbf{C_I}\widetilde{\mathbf{e}}_F + \mathbf{C_P}\dot{\widetilde{\mathbf{e}}}_F + \mathbf{C_D}\ddot{\widetilde{\mathbf{e}}}] - (\mathbf{d}-\hat{\mathbf{d}})^T\boldsymbol{\kappa}\mathbf{J}^T\widetilde{\mathbf{F}}\mathbf{S} \qquad (12)$$

and Eq. (4) is used to expand the derivative of the Lyapunov function,

$$\dot{\mathbf{V}} = \mathbf{S}^T\mathbf{M}[\mathbf{C_I}\widetilde{\mathbf{e}}_F + \mathbf{C_P}\dot{\widetilde{\mathbf{e}}}_F + \mathbf{F}^T\ddot{\mathbf{x}}_{ref} - \mathbf{F}^T\dot{\mathbf{J}}\dot{\mathbf{q}} - \mathbf{F}^T\mathbf{J}\mathbf{M}^{-1}\mathbf{u} + \mathbf{F}^T\mathbf{J}\mathbf{M}^{-1}\mathbf{C}\dot{\mathbf{q}}$$
$$+ 2\dot{\widetilde{\mathbf{F}}}^T\dot{\mathbf{e}} + \ddot{\widetilde{\mathbf{F}}}^T\mathbf{e} + \ddot{\widetilde{\mathbf{h}}}] + \mathbf{S}^T\mathbf{F}^T\mathbf{J}\mathbf{d} - \mathbf{S}^T\mathbf{F}^T\mathbf{J}(\mathbf{d}-\hat{\mathbf{d}}) \qquad (13)$$

Note that $\mathbf{S}^T\boldsymbol{\kappa}\mathbf{F}^T\mathbf{J}\mathbf{d} - \mathbf{S}^T\mathbf{F}^T\mathbf{J}(\mathbf{d}-\hat{\mathbf{d}})$ in Eq. (13) can be rewritten as $\mathbf{S}^T\mathbf{F}^T\mathbf{J}(\mathbf{d}-\hat{\mathbf{d}})(1-\boldsymbol{\kappa})$ and due to the disturbance limits imposed in Eq. (9) becomes $\mathbf{S}^T\mathbf{F}^T\mathbf{J}(\mathbf{d}-\hat{\mathbf{d}})(1-\boldsymbol{\kappa}) \leq \mathbf{0}$. As a result, the following criterion is sufficient to ensure the asymptotic stability ($\dot{\mathbf{V}}(t) < \mathbf{0}$) of Eq. (13):

$$\dot{\mathbf{V}} = \mathbf{S}^T\mathbf{M}[\mathbf{C_I}\widetilde{\mathbf{e}} + \mathbf{C_P}\dot{\widetilde{\mathbf{e}}}_F + \mathbf{F}^T\ddot{\mathbf{x}}_{ref} - \mathbf{F}^T\dot{\mathbf{J}}\dot{\mathbf{q}} - \mathbf{F}^T\mathbf{J}\mathbf{M}^{-1}\mathbf{u} + \mathbf{F}^T\mathbf{J}\mathbf{M}^{-1}\mathbf{C}\dot{\mathbf{q}}$$
$$+ 2\dot{\widetilde{\mathbf{F}}}^T\dot{\mathbf{e}} + \ddot{\widetilde{\mathbf{F}}}^T\mathbf{e} + \ddot{\widetilde{\mathbf{h}}}] + \mathbf{S}^T\mathbf{F}^T\mathbf{J}\hat{\mathbf{d}} = -\mathbf{S}^T\mathbf{K_s}\mathbf{S} \qquad (14)$$

where $\mathbf{K_s} = \mathrm{diag}(K_{s,t}, K_{s,n}, \dots, K_{s,a})$ is a positive definitive diagonal feedback gain matrix to push individual error components onto the sliding surface. Hence, the control law is obtained from Eq. (14) as

$$\mathbf{u} = \begin{bmatrix} u_t \\ u_n \\ u_b \\ u_a \\ u_c \end{bmatrix} = \mathbf{J}^{-1}\mathbf{F}\mathbf{M}[\mathbf{C_I}\widetilde{\mathbf{e}}_F + \mathbf{C_P}\dot{\widetilde{\mathbf{e}}}_F + \mathbf{F}^T\ddot{\mathbf{x}}_{ref} - \mathbf{F}^T\dot{\mathbf{J}}\dot{\mathbf{q}} + 2\dot{\widetilde{\mathbf{F}}}^T\dot{\mathbf{e}} + \ddot{\widetilde{\mathbf{F}}}^T\mathbf{e}$$
$$+ \ddot{\widetilde{\mathbf{h}}}_F + \mathbf{M}^{-1}\mathbf{K_s}\mathbf{S}] + \mathbf{C}\dot{\mathbf{q}} + \hat{\mathbf{d}} \qquad (15)$$

where the disturbance ($\hat{\mathbf{d}}$) is evaluated from Eq. (8).

The asymptotic stability of the tool tip contour controller (Eq. (15)) is guaranteed as follows: The Lyapunov function ($\mathbf{V}$) postulated in Eq. (10) is lower bounded, and its derivative ($\dot{\mathbf{V}}$) is forced to decrease by the condition imposed in Eq. (14). As a result, the sliding surface ($\mathbf{S}$), the contour error states ($\int_0^t\widetilde{\mathbf{e}}_F d\tau, \widetilde{\mathbf{e}}_F, \dot{\widetilde{\mathbf{e}}}_F$), and the estimated disturbances acting on the tool ($\hat{\mathbf{d}}$) are all bounded. The stable sliding surface ($\mathbf{S}$) designed in Eq. (15) is substituted into the contour error dynamics (Eq. (4)) to obtain the following:

$$\dot{\mathbf{S}} + \mathbf{M}\mathbf{K_s}\mathbf{S} = \mathbf{F}^T\mathbf{J}\mathbf{M}^{-1}(\mathbf{d}-\hat{\mathbf{d}}) \qquad (16)$$

Equation (16) proves that $\dot{\mathbf{S}}$ is bounded since ($\mathbf{d}-\hat{\mathbf{d}}$) is bounded, and $\mathbf{J}$, $\mathbf{F}^T$ are both bounded by the reference trajectory. $\ddot{\widetilde{\mathbf{e}}}_F$ is bounded from Eqs. (6) and (16), the second derivative of Lyapunov function (Eq. (14)),

$$\ddot{\mathbf{V}} = -\left(\mathbf{C_P}\widetilde{\mathbf{e}}_F + \mathbf{C_I}\int_0^t\widetilde{\mathbf{e}}_F d\tau + \mathbf{C_D}\dot{\widetilde{\mathbf{e}}}_F\right)(\mathbf{C_P}\dot{\widetilde{\mathbf{e}}}_F + \mathbf{C_I}\widetilde{\mathbf{e}}_F + \mathbf{C_D}\ddot{\widetilde{\mathbf{e}}}_F)$$

$$(17)$$

is also bounded. To conclude, $\mathbf{V}$ is positive definite lower bounded, $\dot{\mathbf{V}}$ is positive definite decreasing, and $\ddot{\mathbf{V}}$ is bounded and this proves that $\dot{\mathbf{V}}$ is a uniformly continuous function. Hence, Barbalat's lemma [20] dictates that $\mathbf{V}\rightarrow\mathbf{0}$, $\mathbf{S}\rightarrow\mathbf{0}$ as $t\rightarrow\infty$, and all the contour errors on the sliding surface converge to origin, $\widetilde{\mathbf{e}}_F \rightarrow\mathbf{0}$, and $\dot{\widetilde{\mathbf{e}}}_F\rightarrow\mathbf{0}$. Considering the simplified homogenous transformation ($\widetilde{\mathbf{e}}_F = \widetilde{\mathbf{F}}^T\mathbf{e}$) between the contour errors ($\widetilde{\mathbf{e}}_F$) and tracking errors ($\mathbf{e}$) from Eq. (3), it yields that both contour and the drive tracking errors converge asymptotically to the origin: $\mathbf{e}\rightarrow\mathbf{0}$ as $\widetilde{\mathbf{e}}_F\rightarrow\mathbf{0}$.

The overall controller structure is illustrated in Fig. 2. Unlike in single input single output (SISO) control structures, the interpolator does not use the inverse kinematics to generate reference com-
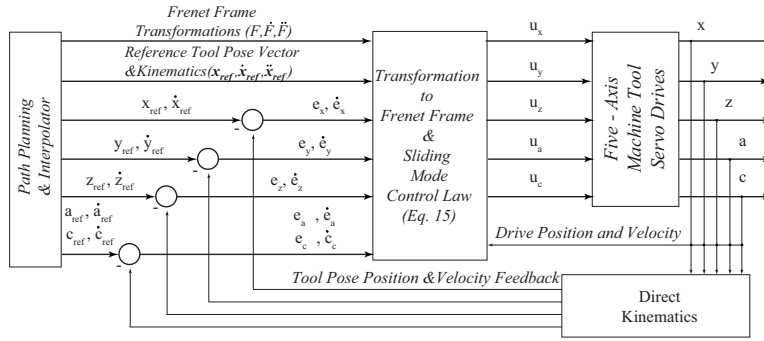
**Fig. 2  Tool tip sliding mode contour controller block diagram**

mands to the drives in the proposed contouring controller. Instead, the interpolator generates the reference tool tip position command in the P (workpiece coordinates) system and the rotary drive positions in the M (machine coordinates) system. The proposed controller uses the pose tracking errors and utilizes Frenet frame transformations to compute the contour error dynamics. The control action is then sent to the five physical drives of the machine tool. As explained in Part I, due to the kinematics of the machine tool, tracking errors of all five axis influence the tool tip position in the P-system. However, the kinematics of the machine tool allows compensation for the tool tip positioning errors by utilizing only the Cartesian axis of the machine tool. The tool position in P-system is used in the contour error estimation and Cartesian axes are coupled together. Since the tool tip contour errors that are directly influenced by the errors in normal and binormal directions $(e_n, e_b)$ are emphasized, higher bandwidths $(\omega_{n,n}, \omega_{n,b})$ and feedback gains can be used to achieve more accurate contouring performance. Dynamics in the tangent direction are set slower so that the drives are not saturated. In contrast, the rotary drives are not coupled during computation of the control action, rather regulated individually. Hence, the above sliding mode controller ensures the stability of the complete machine tool during simultaneous five-axis machining.

**2.2  Design of Sliding Mode Controller for the Tool Orientation Contour Errors.** The orientation contour error is defined as the normal deviation from the orientation trajectory in Part I [19], which is briefly summarized here to derive the control law. The orientation errors defined in spherical coordinates ($\mathbf{e_o} = [e_{o,i}, e_{o,j}, e_{o,k}]^T$) are reflected in the normal direction to the desired tool-path, and the contour errors are estimated as

$$\boldsymbol{\varepsilon_o} = \mathbf{e_o} - \overline{\boldsymbol{\omega}}(\mathbf{e_o} \cdot \overline{\boldsymbol{\omega}}) \qquad (18)$$

where $\overline{\boldsymbol{\omega}} = \boldsymbol{\omega}/|\boldsymbol{\omega}|$ is the normalized angular velocity of the tool axis. Using the orientation Jacobian ($\mathbf{J_O}$) the tool orientation tracking error ($\mathbf{e_o}$) is evaluated from rotary drive tracking errors ($\mathbf{e_R} = [e_a, e_c]^T$) as

$$\mathbf{e_o} \approx \mathbf{J_O} \mathbf{e_R} \qquad (19)$$

The relationship between the tool orientation contour error vector in the P-system ($\boldsymbol{\varepsilon_o}$) and the corresponding rotary drive errors ($\boldsymbol{\varepsilon}_R = [\varepsilon_a, \varepsilon_c]$) in the M-system was obtained as

$$\boldsymbol{\varepsilon_R} = \begin{bmatrix} \varepsilon_a \\ \varepsilon_c \end{bmatrix} = \mathbf{e_R} - \overline{\mathbf{v}}(\overline{\mathbf{v}} \cdot \mathbf{e_R}) \qquad (20)$$

where $\overline{\mathbf{v}} = [\overline{v}_a, \overline{v}_c]^T$ contains normalized rotary drive velocities.

The sliding mode contour controller designed for the tool tip contour control in Sec. 2.1 also sends control signals $(u_a, u_c)$ to minimize individual tracking errors $(e_a, e_c)$ of the rotary drives. However, a separate controller is redesigned in this section for the rotary drives in order to minimize the orientation contour error components $(\varepsilon_a, \varepsilon_c)$ in parallel to the regular tracking errors

$(e_a, e_c)$. By considering only the motion of the rotary drives from Eq. (1), the decoupled tracking error dynamics for rotary drives can be expressed as

$$\ddot{\mathbf{e}}_R = \begin{bmatrix} \ddot{e}_a \\ \ddot{e}_c \end{bmatrix} = \ddot{\mathbf{x}}_{\text{ref}} - \mathbf{M}^{-1}(\mathbf{u} - \mathbf{d} - \mathbf{C}\dot{\mathbf{q}}) \qquad (21)$$

where $\mathbf{M} = \text{diag}(m_a, m_c)$ and $\mathbf{C} = \text{diag}(c_a, c_c)$ contain drive inertias and damping values. Tracking errors of the rotary drives are then redefined as the weighted sum of the regular rotary drive tracking errors ($\mathbf{e_R} = [e_a, e_c]$) and the integral of the contour error components ($\boldsymbol{\varepsilon_R} = [\varepsilon_a, \varepsilon_c]$) from Eq. (18) as

$$\widetilde{\mathbf{e}} = \underbrace{\begin{bmatrix} e_a \\ e_c \end{bmatrix}}_{\mathbf{e_R}} + \underbrace{\begin{bmatrix} w_a & 0 \\ 0 & w_c \end{bmatrix}}_{\mathbf{W}} \int_0^t \underbrace{\begin{bmatrix} \varepsilon_a \\ \varepsilon_c \end{bmatrix}}_{\boldsymbol{\varepsilon_R}} d\tau \qquad (22)$$

where $\mathbf{W} = \text{diag}(w_a, w_c)$ is the positive definitive diagonal weighting matrix. Note that when the weights $(w_a, w_c)$ are set to zero, the new error state ($\widetilde{\mathbf{e}}$) is based only on the tracking errors of rotary drives. As the weights are increased, the effects of contour errors are raised in $\widetilde{\mathbf{e}}$. Consequently, minimizing the new error state with nonzero weight will introduce coupling and synchronization between the rotary drives to improve the contouring performance. Similar to the sliding mode controller design procedure presented in Sec. 2.1, a sliding surface ($\mathbf{S} \in \mathfrak{R}^{2 \times 1}$) that spins over the proposed error states is selected as

$$\mathbf{S} = \boldsymbol{\Delta}\widetilde{\mathbf{e}} + \dot{\widetilde{\mathbf{e}}} = \mathbf{0} \qquad (23)$$

where $\boldsymbol{\Delta} = \text{diag}(\lambda_a, \lambda_c)$ is the desired bandwidth of the errors on the sliding surface. The control input ($\mathbf{u} \in \mathfrak{R}^{2 \times 1}$) is manipulated in such a way that the errors and derivatives converge asymptotically to the stable sliding surface where they eventually slide to the origin. The disturbances ($\mathbf{d} \in \mathfrak{R}^{2 \times 1}$) are estimated from the following observer:

$$\dot{\hat{\mathbf{d}}} = \boldsymbol{\Gamma}\boldsymbol{\kappa}\mathbf{S} \rightarrow \hat{\mathbf{d}}(k) = \hat{\mathbf{d}}(k-1) + T\boldsymbol{\Gamma}\boldsymbol{\kappa}\mathbf{S} \qquad (24)$$

where $\boldsymbol{\Gamma} \in \mathfrak{R}^{2 \times 2}$ contains parameter adaptation gains, and $\boldsymbol{\kappa} \in \mathfrak{R}^{2 \times 2}$ is used to keep the observed disturbance within the given boundaries similar to the expression presented in Eq. (9). In order to push the errors onto the sliding surface, a positive definite lower bounded Lyapunov function is used,

$$V = \frac{1}{2}(\mathbf{S^T M S} + (\mathbf{d} - \hat{\mathbf{d}})^T \boldsymbol{\Gamma}^{-1}(\mathbf{d} - \hat{\mathbf{d}})) \qquad (25)$$

and the asymptotic stability ($\dot{V}(t) < 0$) is ensured by setting

$$\mathbf{S^T M}[\boldsymbol{\Delta}\dot{\widetilde{\mathbf{e}}} + \ddot{\mathbf{x}}_{\text{ref}} - \mathbf{M}^{-1}(\mathbf{u} - \mathbf{d} - \mathbf{C}\dot{\mathbf{q}}) + \mathbf{W}\dot{\boldsymbol{\varepsilon}}_R] = -\mathbf{S^T K_s S} \qquad (26)$$

where $\mathbf{K_s} = \text{diag}(K_{s,a}, K_{s,c})$ is the feedback gain matrix. The control law is obtained from Eqs. (21), (22), and (26) as
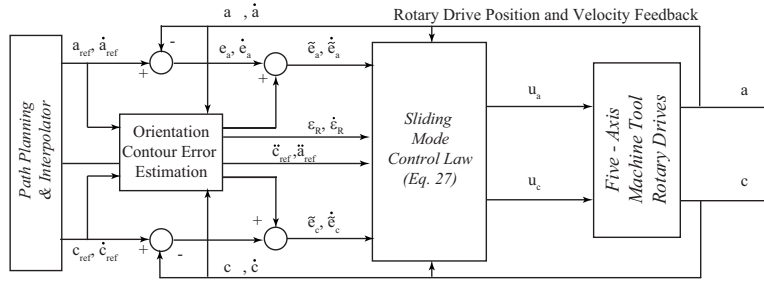
**Fig. 3  Tool orientation contour controller**

$$\mathbf{u} = \begin{bmatrix} u_a \\ u_c \end{bmatrix} = \mathbf{M}\boldsymbol{\Delta}\dot{\tilde{\mathbf{e}}} + \mathbf{M}\ddot{\mathbf{x}}_{\mathbf{ref}} + \mathbf{C}\dot{\mathbf{q}} + \mathbf{MW}\dot{\boldsymbol{\varepsilon}}_{\mathbf{R}} + \hat{\mathbf{d}} + \mathbf{K}_s\mathbf{S} \quad (27)$$

The proposed control law minimizes the error state that contains weighted sum of tracking and the contour components, $\tilde{\mathbf{e}} = \mathbf{e}_R + \mathbf{W}\int_0^t \boldsymbol{\varepsilon}_\mathbf{R} d\tau$. The block diagram of the orientation contour controller is presented in Fig. 3.

Stability of the orientation controller (Eq. (27)) is studied similar to the one presented for the tool tip position controller. Since the derivative of Lyapunov function postulated in Eq. (25) is decreasing and $\mathbf{S}$, $\tilde{\mathbf{e}}$, $\dot{\tilde{\mathbf{e}}}$, and $\hat{\mathbf{d}}$ are all bounded, this implies that the signals $\mathbf{e}_\mathbf{R}$, $\dot{\mathbf{e}}_\mathbf{R}$ and $\int \boldsymbol{\varepsilon}_\mathbf{R}$, $\boldsymbol{\varepsilon}_\mathbf{R}$ are also bounded with respect to Eq. (22). Control ($\mathbf{u}$) from Eq. (27) is substituted into Eq. (21) to obtain

$$\dot{\mathbf{S}} + \mathbf{M}^{-1}\mathbf{K}_s\mathbf{S} = \mathbf{M}^{-1}(\mathbf{d}\text{-}\hat{\mathbf{d}}) \quad (28)$$

which shows that $\dot{\mathbf{S}}$ and $\ddot{\tilde{\mathbf{e}}}$ are bounded functions. Using Eq. (21) and the conclusions drawn from Eq. (28), the boundness of $\ddot{\mathbf{V}}$ is proven. Thus, $\dot{\mathbf{V}}$ is uniformly continuous, and Barbalat's lemma [20] implies that as $t \to \infty$, $\mathbf{V} \to 0$, and $\mathbf{S} \to 0$ proving that the proposed error state converges to origin, $\tilde{\mathbf{e}} \to 0$, and $\dot{\tilde{\mathbf{e}}} \to 0$ and the controller is stable.

Since the Cartesian axis positions do not influence the tool orientation, the tool axis orientation controller works as an uncoupled system. The contour error weight ($\mathbf{W}$) specifies the amount of coupling introduced between the rotary axes. If $\mathbf{W} = \text{diag}(0,0)$, the MIMO sliding mode control law in Eq. (27) is reduced down to two separate stable SISO SMC laws for tracking control of $a$ and $c$ rotary drives. On the other hand, the effect of nonzero weights for the orientation contouring performance is investigated as follows: When the states are away from the sliding surface ($\mathbf{S}$) the feedback term ($\mathbf{K}_s\mathbf{S}$) is nonzero, which pushes the states back to the surface. When the error states are on the sliding surface ($\mathbf{K}_s\mathbf{S} = 0$) during steady state, the disturbance estimation term can be neglected, and the equivalent control is obtained from Eq. (27) as

$$\mathbf{u} = \mathbf{M}\boldsymbol{\Delta}\dot{\tilde{\mathbf{e}}} + \mathbf{M}\ddot{\mathbf{x}}_{\text{ref}} + \mathbf{C}\dot{\mathbf{q}} + \mathbf{MW}\dot{\boldsymbol{\varepsilon}}_{\mathbf{R}} \quad (29)$$

Let us substitute the equivalent control ($\mathbf{u}$) from Eq. (29) into the error dynamics presented in Eq. (21) to obtain the steady state tracking errors ($\mathbf{e}_\mathbf{R}$) of the drives

$$\ddot{\mathbf{e}}_\mathbf{R} = \ddot{\mathbf{x}}_{\text{ref}} - \mathbf{M}^{-1}(\mathbf{M}\boldsymbol{\Delta}\dot{\tilde{\mathbf{e}}} + \mathbf{M}\ddot{\mathbf{x}}_{\text{ref}} + \mathbf{MW}\dot{\boldsymbol{\varepsilon}}_\mathbf{R}) \quad (30)$$

which can be further simplified by substituting the expression for $\dot{\tilde{\mathbf{e}}}$ from Eq. (22), and rewriting it in Laplace ($s$) domain yields

$$s(s + \boldsymbol{\Delta})\mathbf{I}\mathbf{e}_\mathbf{R}(s) = -(s + \boldsymbol{\Delta})\mathbf{IW}\boldsymbol{\varepsilon}_\mathbf{R}(s)$$

$$\mathbf{e}_\mathbf{R}(s) = -\mathbf{W}\frac{\boldsymbol{\varepsilon}_\mathbf{R}(s)}{\mathbf{I}s} \quad (31)$$

where $\mathbf{I}_{2\times2}$ is identity matrix. When assuming that there is no contour error ($\mathbf{W} = \text{diag}(0,0)$) added to the rotary drive tracking errors, $\mathbf{e}_\mathbf{R}^*$ is denoted as the pure rotary drive tracking errors without the effect of contour coupling. Equation (31) can be re-expressed to relate the drive tracking errors between the coupled ($\mathbf{e}_\mathbf{R}$) and the uncoupled ($\mathbf{e}_\mathbf{R}^*$) cases,

$$\mathbf{e}_\mathbf{R}(s) = \mathbf{e}_\mathbf{R}^*(s) - \mathbf{W}\frac{\boldsymbol{\varepsilon}_\mathbf{R}(s)}{\mathbf{I}s} \quad (32)$$

Similarly, Eq. (18) can be rewritten for the coupled ($\boldsymbol{\varepsilon}_\mathbf{R}$) and the uncoupled ($\boldsymbol{\varepsilon}_\mathbf{R}^*$) cases as

$$\boldsymbol{\varepsilon}_\mathbf{R} = \mathbf{e}_\mathbf{R} - \bar{\mathbf{v}}(\bar{\mathbf{v}} \cdot \mathbf{e}_\mathbf{R})$$
$$\boldsymbol{\varepsilon}_\mathbf{R}^* = \mathbf{e}_\mathbf{R}^* - \bar{\mathbf{v}}(\bar{\mathbf{v}} \cdot \mathbf{e}_\mathbf{R}^*) \quad (33)$$

Hence, substituting Eq. (33) into Eq. (32) leads to

$$\boldsymbol{\varepsilon}_\mathbf{R} + \bar{\mathbf{v}}[\bar{\mathbf{v}} \cdot (\mathbf{e}_R^* - \mathbf{e}_\mathbf{R})] = \boldsymbol{\varepsilon}_\mathbf{R}^* - \mathbf{W}\frac{\boldsymbol{\varepsilon}_\mathbf{R}}{\mathbf{I}s} \quad (34)$$

and substituting $\mathbf{e}_\mathbf{R}^*(s) - \mathbf{e}_\mathbf{R}(s) = \mathbf{W}(\boldsymbol{\varepsilon}_\mathbf{R}(s)/s)$ from Eq. (32) into Eq. (34) yields

$$\boldsymbol{\varepsilon}_\mathbf{R}(s) + \bar{\mathbf{v}}[\bar{\mathbf{v}} \cdot \boldsymbol{\varepsilon}_\mathbf{R}(s)] = \boldsymbol{\varepsilon}_\mathbf{R}^*(s) - \mathbf{W}\frac{\boldsymbol{\varepsilon}_\mathbf{R}(s)}{\mathbf{I}s} \quad (35)$$

Note that the contour error vector and the angular velocity vector are perpendicular [19], $\boldsymbol{\omega} \cdot \boldsymbol{\varepsilon}_\mathbf{R} = 0 \to \mathbf{v} \cdot \boldsymbol{\varepsilon}_\mathbf{R} = 0$; therefore, Eq. (35) can be simplified as

$$\boldsymbol{\varepsilon}_\mathbf{R}(s) = \frac{\mathbf{I}s}{\mathbf{I}s + \mathbf{W}}\boldsymbol{\varepsilon}_\mathbf{R}^*(s) \quad (36)$$

Hence, Eq. (36) shows that for positive definitive weight matrix ($\mathbf{W}$), the controller minimizes the contour errors in the coupled mode ($\boldsymbol{\varepsilon}_\mathbf{R}$) as compared with the uncoupled initial case ($\boldsymbol{\varepsilon}_\mathbf{R}^*$) especially at low frequency range. In parallel, the stability of the tracking errors ($\mathbf{e}_\mathbf{R}$) for the coupled case can be studied by substituting Eq. (33) into Eq. (32):

$$\mathbf{e}_\mathbf{R}(s) = \mathbf{e}_\mathbf{R}^*(s) - \frac{\mathbf{W}}{\mathbf{I}s}[\mathbf{e}_\mathbf{R}(s) - \bar{\mathbf{v}}[\bar{\mathbf{v}} \cdot \mathbf{e}_\mathbf{R}(s)]] \quad (37)$$

which is simplified as

$$\mathbf{e}_\mathbf{R}(s) = \mathbf{e}_\mathbf{R}^*(s) - \frac{\mathbf{W}}{\mathbf{I}s}[\Psi \cdot \mathbf{e}_\mathbf{R}(s)] \leftarrow \Psi = \begin{bmatrix} 1 - \bar{v}_a & -\bar{v}_a\bar{v}_c \\ -\bar{v}_a\bar{v}_c & 1 - \bar{v}_c \end{bmatrix}$$
$$(38)$$

where $\Psi$ has positive semidefinite eigenvalues. Equation (38) is reorganized to obtain the transfer function of tracking errors ($\mathbf{e}_\mathbf{R}$) in the coupled case:
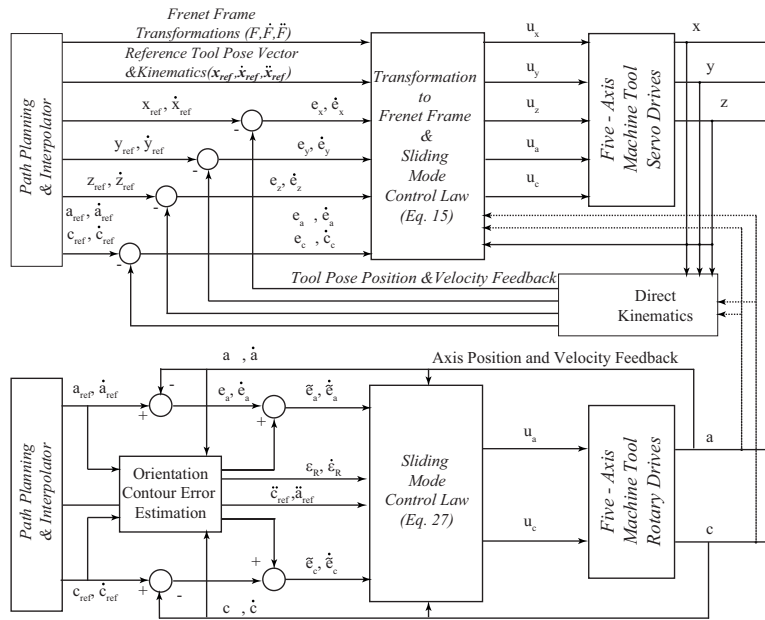
**Fig. 4  Complete five-axis contour controller block diagram**

$$\mathbf{e_R}(s) = \frac{-\mathbf{I}s}{\mathbf{I}s + \mathbf{W}\Psi}\mathbf{e_R^*}(s) \tag{39}$$

which is stable for positive contour weights ($\mathbf{W}$).

The complete five-axis contour controller is obtained by combining the tool tip controller presented in Sec. 2.1 with the tool orientation contour controller, as shown in the block diagram given in Fig. 4. As presented in Sec. 2.2 and also illustrated in Fig. 4, the orientation contour controller is strictly uncoupled from the Cartesian contour controller and requires feedback only from the rotary drives. The stability study has shown that the orientation controller is stable and both contour and tracking error signals are bounded. The tool tip contour controller uses position and velocity feedback from the rotary drives in the computation of the Jacobian matrix ($\mathbf{J}$) and in the inverse kinematics transformation. The tool tip controller is internally bounded input-output stable, and the signals required from the rotary drives are all bounded allowing the tool tip controller to generate bounded control to the Cartesian drives. As a result, the overall five-axis contour control system is stable.

## 3  Implementation and Experimental Results

The open architecture controlled experimental five-axis machine tool is presented in Part I [19], and its dynamic parameters are given in Table 1. This section compares the five-axis contouring performance of the proposed contour controller against the SISO axis based sliding mode tracking controller [9].

The SMC of each drive is tuned separately, and the bandwidths of the Cartesian axis are matched in order to obtain better contouring performance (see Table 2). Previously presented five-axis contour tool-path (see Fig. 5) is used in air-cutting tests. A smooth trajectory is generated with a maximum cruise speed of 50 mm/s and cubic acceleration/decelerations of 1500 mm/s$^2$. Correspond-

ing axis reference position and velocity commands are shown in Fig. 6. It should be noted that although the tangential feedrate is selected conservatively, higher reference axis velocities and accelerations are observed because of the continuously varying path curvature and the kinematics of the machine tool. As shown in Fig. 6($c$), $y$ and $z$ axis are commanded as high as 200 mm/s and 90 mm/s, respectively. Experimental air-cutting results under SISO sliding mode control is presented are Fig. 7. Tracking errors are measured by comparing the reference axis trajectory against the actual positions measured from rotary encoders mounted at the motor side of each drive. As shown on Figs. 7($b$)–7($f$), dedicated SMCs with disturbance observers provide each axis to accurately track their reference position commands. Highest axis tracking errors are observed as $\max(e_x)=15~\mu$m, $\max(e_y)=13~\mu$m, $\max(e_z)=7~\mu$m, $\max(e_a)=2.2$ mrad, and $\max(e_c)=1.7$ mrad. By inspecting the velocity trajectory of the drives from Figs. 6($c$) and 6($d$), it can be observed that peak tracking errors occur especially at the velocity reversal of the axis where Coulomb friction acts as a step disturbance to the drives. The contour error estimation method presented by Erkorkmaz and Altintas [15] is then used to measure the tool tip contour error along the tool-path and presented in Fig. 7($a$). Precise axis tracking performance does not always guarantee the desired contouring accuracy during simultaneous five-axis contour machining. Since tracking errors of all drives affect the tool position, the mean absolute tool tip contour error is calculated as $\text{mean}(\varepsilon)=45~\mu$m and the maximum is $\max(\varepsilon)=317~\mu$m. It should also be noted that the main contribution to the contour errors are originated from the tracking errors of $a$ and $c$ rotary drives. Both axes rotate the workpiece, and due to the offset between the rotary drives' axis of rotations and the placement of the workpiece coordinate system, small rotations may cause large deviation of the tool tip on the workpiece. The peak errors are observed in tool tip contouring (Fig. 7($a$)) pro-

**Table 2  Five-axis SMC parameters (SISO scheme)**

| SMC parameters | $x$-axis | $y$-axis | $z$-axis | $a$-axis | $c$-axis |
|---|---|---|---|---|---|
| $\omega_n$(rad/s) | 200 | 200 | 180 | 150 | 200 |
| $K_s$ (V mm/s) (V rad/s for rotary drives) | 7 | 5 | 5 | 0.5 | 1 |
| Disturbance adaptation gain $\Gamma$ (V/mm(or rad)) | 25 | 30 | 15 | 3 | 3 |

a) Reference Tool Tip (Pref=[Px,Py,Pz]) Path     b) Reference Tool Axis Orientation Path
(Oref=[Oi,Oj,Ok])
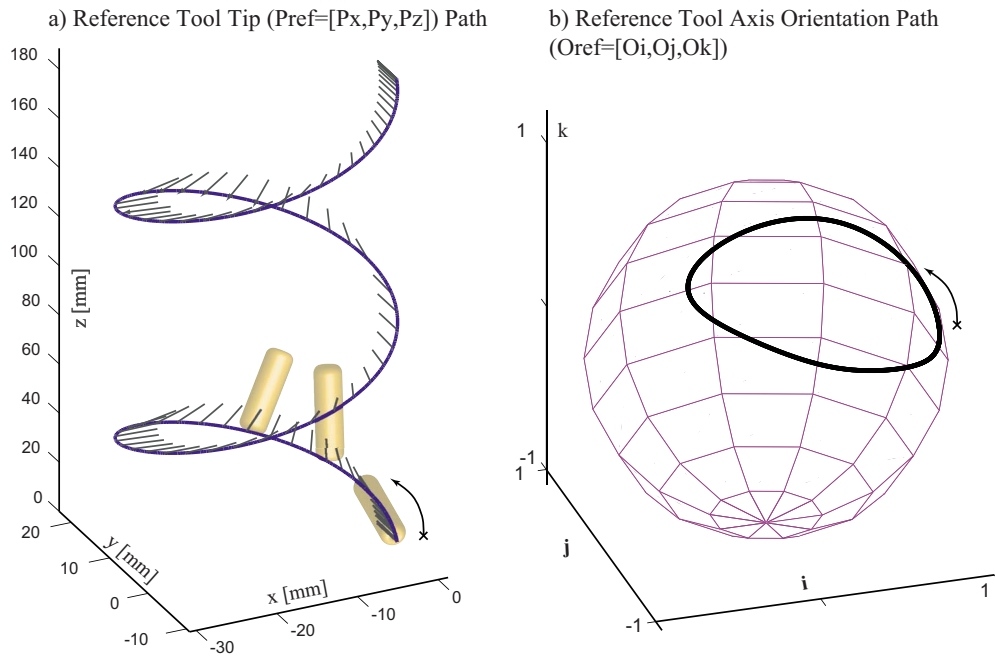


Fig. 5   Five-axis test tool-path

nominally when the *a* drive shows its highest tracking error lag during velocity reversals (Fig. 7(*e*)). The peak error points are identified in Part I at locations ∼1 s, 2.2 s, 3.5 s, and 5 s. Smaller peaks are also observed (∼1.5 s, 3 s, 3.5 s, and 4.2 s), which are related to the tracking errors of the *c* axis. Thus, faster dynamics on the rotary axes are desired, or improved coordination between the drives should be accomplished in the CNC's control law to minimize tool tip contour errors.

The following experiments are performed using the proposed tool tip contour controller scheme shown in Fig. 4. The tool tip contour controller couples Cartesian axes together for minimizing the tool tip contour errors. The rotary drives are controlled as SISO systems where their individual tracking errors are minimized by setting the coupling weights to zero ($w_a = w_c = 0$). The parameters for the tangential, normal, and binormal directions are tuned and represented in Table 3. The tangential direction is tuned slower so that higher gains in the normal and binormal directions are achieved without causing saturation of the drives. The experimental contouring results are presented in Fig. 8. Since the rotary drives are not coupled, they demonstrate identical tracking performance as in the previous SISO case (see Figs. 7, 8(*e*), and 8(*f*)). In contrast, due to the contour objective of the proposed controller,
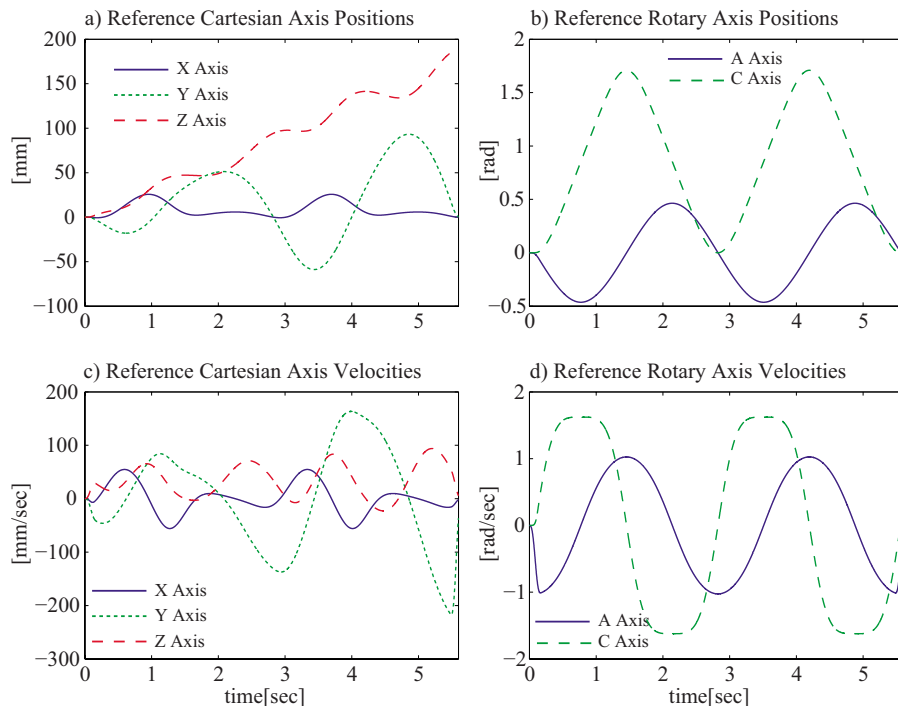


Fig. 6   Reference axis trajectories
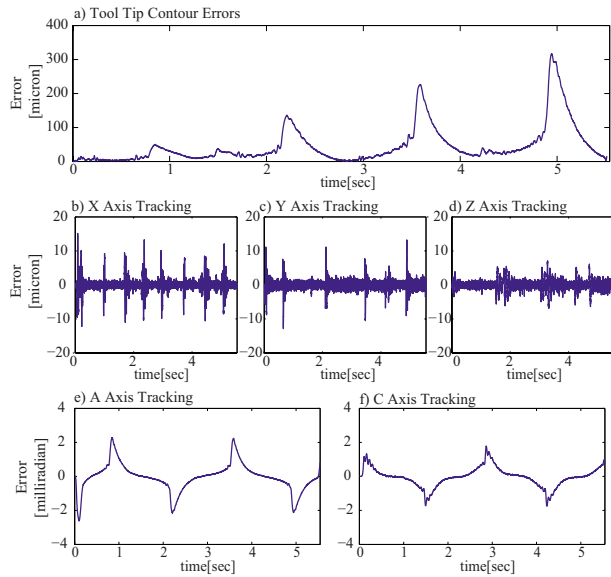
Fig. 7 Contouring performance of the SISO controller



Fig. 8 Contouring performance of the proposed controller

the Cartesian axes are now coupled and demonstrate higher axis tracking errors $\max(e_x)=130$ $\mu$m, $\max(e_y)=216$ $\mu$m, and $\max(e_z)=130$ $\mu$m (see Figs. 8(b)–8(d)). Peaks in tracking error occur particularly when the rotary drives exhibit their highest errors. This indicates that the Cartesian drives are deviating from their reference trajectory in order to compensate against the deviation of the tool tip from desired contour. As a result, improved contouring performance is achieved, as shown in Fig. 8(a). The mean tool tip contour error is calculated as $\text{mean}(\varepsilon)=10$ $\mu$m, which is approximately four times lower in comparison to the SISO case, and the maximum deviation is reduced from 317 $\mu$m down to $\max(\varepsilon)=79$ $\mu$m. Tests are also performed at higher feedrates where similar contouring performance trend is observed (see Table 4). Furthermore, the power consumption and aggressiveness of SISO against the proposed contour SMC are compared for the same trajectory. Control signal sent to amplifiers of Cartesian drives from both controllers are presented in Fig. 9. Both control schemes generate control signal well within the limits of the amplifiers ($\pm 5$ V), and the proposed contour controller demonstrates very similar characteristic in terms of aggressiveness and power consumption.

In order to study the effects of the tuning parameters at fixed feedrate (60 mm/s), the tangential, normal, and binormal bandwidth parameters are varied, and the results are summarized in Table 5. In the first test, the bandwidth in tangent direction is set to $\omega_{n,t}=100$ rad/s where the normal and binormal bandwidths are reduced from 230 rad/s down to 200 rad/s. As compared in Table 5, the maximum and mean contour errors are increased from 90 $\mu$m to 115 $\mu$m and from 13 $\mu$m to 18 $\mu$m, respectively. On the other hand, as the tangential bandwidth is varied from 100 rad/s to 70 rad/s, for the same normal and binormal bandwidths, tool tip contour errors do not show any significant change validating that the tangent bandwidth component has little effect on the
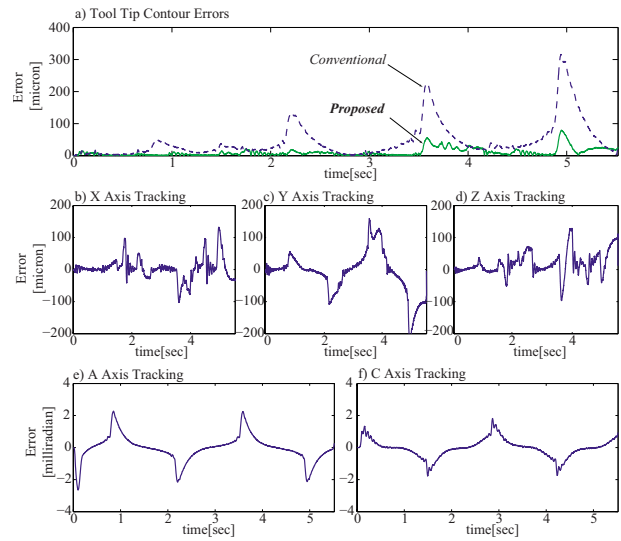
contouring performance due to accurate contour error estimation (see Fig. 10). Hence, normal and binormal bandwidths and gains are the most essential tuning parameters for the proposed controller. Once the equivalent mass and viscous friction values of the drives are identified (Table 1), bandwidth, feedback, and the disturbance adaption gains for each axis can be individually tuned to achieve desired tracking performance in a SISO control scheme; in contrast, proposed SMC controller requires tuning of the coupled gains. From a practical perspective, the control parameters in the normal and binormal directions should be set identical and 10–20% higher than the values set for the slowest drive in the SISO scheme. The tangential bandwidth is then set $\sim$50% lower than the normal direction. Once a working parameter set is obtained, it can be fine-tuned along a simultaneous five-axis contouring path.

As presented in Part I, the orientation contour error is measured as the normal angular deviation from the desired tool-path using

$$\phi_\varepsilon = \cos^{-1}\left(\left(\mathbf{O_{ref}} - \frac{\boldsymbol{\omega}}{|\vec{\boldsymbol{\omega}}|}\frac{\mathbf{e_o}\cdot\boldsymbol{\omega}}{|\vec{\boldsymbol{\omega}}|}\right)\cdot\mathbf{O}\right) \qquad (40)$$

The performance of the proposed orientation contour controller (Eq. (27)) is studied by increasing the coupling weights ($\mathbf{W}=\text{diag}(w_a, w_v)$). By increasing the coupling weights, components from the orientation contour errors are transformed and added to the regular tracking errors of the $a$ and $c$ rotary drives. Thus, rotary axis tracks a compensated reference trajectory, which practically pushes the tool normal to the reference contour, thus penalizing the tool orientation errors. Equation (40) can be used to plot the orientation contour error trend, and the experimental air-cutting results with four different weights, as summarized in Fig. 11. In the first case ($\mathbf{W}=\text{diag}(0,0)$) and there is no coupling between the rotary drives. $a$ and $c$ drives track their individual reference position commands as in the SISO case. As the weights are increased ($\mathbf{W}=\text{diag}(3,3)$, $\mathbf{W}=\text{diag}(4,4)$, and $\mathbf{W}=\text{diag}(5,5)$) at

Table 3 Five-axis contour controller parameters

| SMC parameters | Tangential direction | Normal direction | Binormal direction | $a$-axis | $c$-axis |
|---|---|---|---|---|---|
| $\omega_n$(rad/s) | 100 | 230 | 230 | 150 | 200 |
| $K_s$ (V mm/s) (V rad/s for rotary drives) | 2 | 4 | 4 | 0.5 | 1 |
| Disturbance adaptation gain $\Gamma$ (V/mm(or rad)) | 10 | 20 | 20 | 3 | 3 |
| $w_a, w_c$ (orientation contour error weights W=diag($w_a, w_c$)) | | | | 0 | 0 |

**Table 4  Performance of the proposed controller at different feedrates**

| Tangential feedrate (mm/s) | Five-axis contour controller | | SISO tracking controller | |
|---|---|---|---|---|
| | Max tool tip contour error (mm) | Mean tool tip contour (mm) | Max tool tip contour error (mm) | Mean tool tip contour error (mm) |
| 50 | 0.079 | 0.010 | 0.317 | 0.045 |
| 60 | 0.087 | 0.014 | 0.359 | 0.055 |
| 80 | 0.101 | 0.020 | 0.412 | 0.074 |
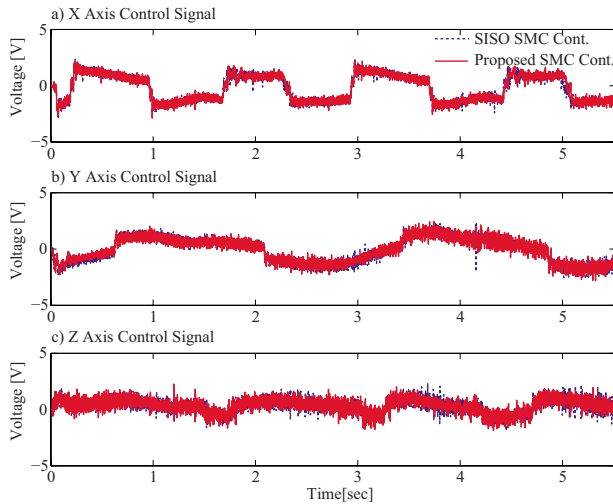


**Fig. 9  Comparison of control signal voltages**

each air-cutting test, rotary drive tracking errors are modified with respect to Eq. (22) to accommodate additional contour error components. As mentioned, this has the effect of modifying the tool-path to compensate the orientation contour errors. The results are summarized in Fig. 11(*a*). As the weights are increased, more coupling is achieved and a steady decline in the orientation contour errors is emphasized in Fig. 11(*b*).

## 4  Conclusion

The objective of five-axis machine tool control is to minimize the tool tip and orientation contour errors. The conventional five-axis control schemes are entirely based on entirely eliminating the tracking errors of the individual axis and take neither the tool-path nor the kinematics of the actual machine tool into consideration. The desired accuracy may not be achieved at high speed contouring of curved paths even if high performance robust controllers are utilized for the drive control. This paper presents a new approach where all five axes of the machine tool are controlled simultaneously by a robust, multi-input–multi-output sliding mode control that incorporates the kinematics of the machine tool. The experimental results show that significant improvement in

**Table 5  The effect of directional bandwidths on the proposed controller's performance**

| Bandwidths (rad/s) | | | Maximum tool tip contour error ($\mu$m) | Mean tool tip contour error ($\mu$m) |
|---|---|---|---|---|
| Tangent | Normal | Binormal | | |
| 100 | 230 | 230 | 90 | 13 |
| 100 | 200 | 200 | 115 | 18 |
| 70 | 230 | 230 | 93 | 12 |
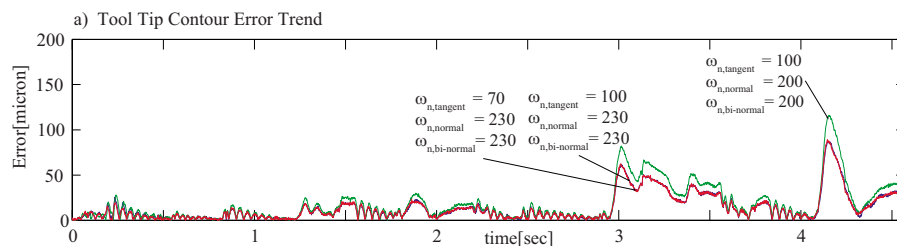


**Fig. 10  Contouring performance with different bandwidths**
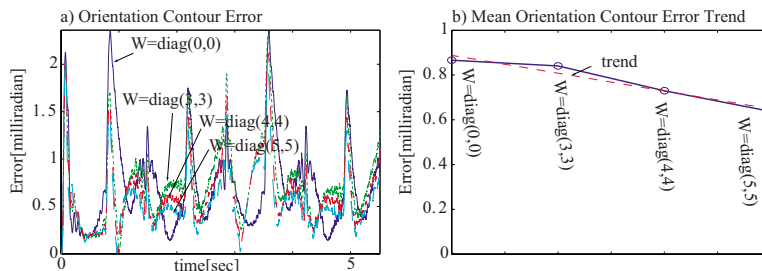


**Fig. 11  Orientation contour controller performance ($F=50$ mm/s)**

contouring performance is achieved at low and at high speed five axis contouring. The added computation load can be handled by employing recent high speed digital signal processors. The algorithm can also be switched between single and multi-axis modes along the tool-path to improve rapid positioning of the tool in air-cutting motions.

## Acknowledgment

## References

[1] Koren, Y., 1992, "Advanced Controllers for Feed Drives," CIRP Ann., **41**(2), pp. 689–698.

[2] Astrom, K., and Wittenmark, B., 1997, *Computer-Controlled Systems: Theory and Design*, 3rd ed., Prentice-Hall, Englewood Cliffs, NJ.

[3] Tomizuka, M., 1987, "Zero Phase Error Tracking Algorithm for Digital Control," ASME J. Dyn. Syst., Meas., Control, **109**, pp. 65–68.

[4] Tung, E. D., and Tomizuka, M., 1993, "Feedforward Tracking Controller Design Based on the Identification of Low Frequency Dynamics," ASME J. Dyn. Syst., Meas., Control, **115**(3), pp. 348–356.

[5] Tsao, T.-C., and Tomizuka, M., 1987, "Adaptive Zero Phase Error Tracking Algorithm for Digital Control," ASME J. Dyn. Syst., Meas., Control, **109**(4), pp. 349–354.

[6] Utkin, V. I., 1977, "Variable Structure Systems With Sliding Modes," IEEE Trans. Autom. Control, **22**(2), pp. 212–222.

[7] Slotine, J.-J. E., and Li, W., 1988, "Adaptive Manipulator Control: A Cast Study," IEEE Trans. Autom. Control, **33**(11), pp. 995–1003.

[8] Stepanenko, Y., Cao, Y., and Su, C.-Y., 1998, "Variable Structure Control of Robotic Manipulator With PID Sliding Surfaces," Int. J. Robust Nonlinear Control, **8**(1), pp. 79–90.

[9] Altintas, Y., Erkorkmaz, K., and Zhu, W.-H., 2000, "Sliding Mode Controller Design for High Speed Feed Drives," CIRP Ann., **49**(1), pp. 265–270.

[10] Rodriguez-Angeles, A., and Nijmeijer, H., 2004, "Synchronizing Tracking Control for Flexible Joint Robots Via Estimated State Feedback," ASME J. Dyn. Syst., Meas., Control, **126**(1), pp. 162–172.

[11] Su, Y., Sun, D., Ren, L., and Mills, J. K., 2006, "Integration of Saturated PI Synchronous Control and PD Feedback For Control of Parallel Manipulators," IEEE Trans. Robot., **22**(1), pp. 202–207.

[12] Ren, L., Mills, J. K., and Sun, D., 2006, "Adaptive Synchronized Control for a Planar Parallel Manipulator: Theory and Experiments," ASME J. Dyn. Syst., Meas., Control, **128**(4), pp. 976–979.

[13] Koren, Y., and Lo, C.-C., 1980, "Cross-Coupled Biaxial Computer Control for Manufacturing Systems," ASME J. Dyn. Syst., Meas., Control, **102**, pp. 265–272.

[14] Koren, Y., and Lo, C.-C., 1991, "Variable-Gain Cross Coupling Controller for Contouring," CIRP Ann., **40**(1), pp. 371–374.

[15] Erkorkmaz, K., and Altintas, Y., 1998, "High Speed Contouring Control Algorithm for CNC Machine Tools," *Proceedings of the ASME Dynamic Systems and Control Division*, ASME International Mechanical Engineering Congress and Exposition, DSC 64, pp. 463–469.

[16] Chiu, G. T.-C., and Tomizuka, M., 2001, "Contouring Control of Machine Tool Feed Drive Systems: A Task Coordinate Frame Approach," IEEE Trans. Control Syst. Technol., **9**(1), pp. 130–139.

[17] Peng, C.-C., and Chen, C.-L., 2007, "Biaxial Contouring Control With Friction Dynamics Using a Contour Index Approach," Int. J. Mach. Tools Manuf., **47**(10), pp. 1542–1555.

[18] Chen, S.-L., Liu, H.-L., and Ting, S. C., 2002, "Contouring Control of Biaxial Systems Based on Polar Coordinates," IEEE/ASME Trans. Mechatron., **7**(3), pp. 329–345.

[19] Sencer, B., Altintas, Y., and Croft, E., 2009, "Modeling and Control of Contouring Errors for Five-Axis Machine Tools—Part I: Modeling," ASME J. Manuf. Sci. Eng., **131**(3), p. 031006.

[20] Slotine, J.-J., and Li, W., 1991, *Applied Nonlinear Control*, Prentice-Hall, Englewood Cliffs, NJ.